Entropy engineering and tunable magnetic order in the spinel high entropy oxide

Graham H.J. Johnstone,[1,2] Mario U. González-Rivas,[1,2] Keith M. Taddei,[3] Ronny Sutarto,[4] George A. Sawatzky,[1,2] Robert J. Green,[5,2] Mohamed Oudah,[1,2] and Alannah M. Hallas[1,2]

[1]*Department of Physics & Astronomy, University of British Columbia, Vancouver, BC V6T 1Z1, Canada*
[2]*Stewart Blusson Quantum Matter Institute, University of British Columbia, Vancouver, BC V6T 1Z4, Canada*
[3]*Neutron Scattering Division, Oak Ridge National Laboratory, Oak Ridge, Tennessee 37831, USA*
[4]*Canadian Light Source; Saskatoon, Saskatchewan S7N 2V3, Canada*
[5]*Department of Physics and Engineering Physics, University of Saskatchewan, Saskatoon, SK S7N 5E2, Canada*

Spinel oxides are an ideal setting to explore the interplay between configurational entropy, site selectivity, and magnetism in high entropy oxides. In this work we characterize the magnetic properties of $(Cr,Mn,Fe,Co,Ni)_3O_4$ and study the evolution of its magnetism as a function of non-magnetic gallium substitution. Across the range of compositions studied here, from 0% to 40% Ga, magnetic susceptibility and powder neutron diffraction measurements show that ferrimagnetic order is robust in the spinel HEO. However, we also find that the ferrimagnetic order is highly tunable and varies significantly in ordering temperature, saturated and sublattice moments, and magnetic hardness. Through x-ray absorption and magnetic circular dichroism, we are able to correlate this tunable magnetic state with strong site selectivity between the various cations and the tetrahedral and octahedral sites in the spinel structure. In particular, we find that while Ni and Cr are largely unaffected by the substitution with Ga, the occupancies of Mn, Co, and Fe are redistributed in response to Ga substitution. Ga substitution also requires an overall reduction in the transition metal valence and this is entirely accommodated by Mn. Finally, we show that while site selectivity has an overall suppressing effect on the configurational entropy, over a certain range of compositions, Ga substitution yields a striking increase to the configurational entropy and may confer additional stabilization. Spinel oxides can be tuned seamlessly from the low entropy to the high entropy regime, making this an ideal platform for entropy engineering.

I. INTRODUCTION

Since their initial discovery in 2015 [1], the rapidly growing field of high entropy oxides (HEOs) has attracted significant interest from chemists, physicists, and materials scientists alike. There is no universally agreed upon definition for what constitutes a high entropy oxide, but in general terms they are crystalline oxides with a high degree of configurational entropy due to the solid solution of multiple (in many cases five) metal cations sharing a single sublattice [2–6]. In certain cases, this configurational entropy is so large that it dominates the free energy landscape at the high temperatures where materials synthesis occurs, such that the resulting single phase solid solution is actually selected by entropic rather than enthalpic forces. HEOs have been demonstrated to have highly tunable properties and enhanced structural stability which lends credence to the idea that they may one day find widespread use in applications such as reversible energy storage [7–9] or catalysis [10]. One question that has elicited significant interest is the degree to which the ideal configurational disorder is actually achieved in real high entropy oxides or whether it is significantly reduced due to short-range ordering or clustering, and the extent to which these effects might alter the structural, magnetic, and electronic properties.

The cubic spinel family of materials, with the general chemical formula AB_2O_4 [11, 12], provide a particularly interesting setting in which to explore the interplay between configurational disorder and structure-function relationships in HEOs. First, the spinel structure offers not one but two cation sublattices: the tetrahedrally coordinated A site that forms a diamond lattice and the octahedrally coordination B site that forms a pyrochlore lattice. In the extreme limit where both sublattices are occupied by a mixture of cations a dramatic enhancement to configurational entropy can be expected. Spinels can also exist as both normal (valence ordered) or inverted (mixing of valences between A and B site) [13, 14], they are known to exhibit oxygen vacancies [12, 15, 16], and they are susceptible to short-range cation ordering [17, 18]. Each of these factors could enhance or diminish the overall degree of configurational entropy. In fact, the notion of entropy stabilization in spinels vastly predates the concept of HEOs in the modern sense. For example, in a series of papers, Navrotsky *et al.* show that even for binary spinel systems such as $MgAl_2O_4$, mixing of the cation sites provides the necessary configurational entropy to stabilize the spinel phase in relation to the component oxide phases, which are favored by enthalpy [19–21].

The spinel family also offers a rich opportunity to study the intersection of magnetism with high configurational disorder. Previous studies on the prototypical rock salt HEO, (Mg,Co,Ni,Cu,Zn)O, have revealed that long range antiferromagnetic order can occur in high entropy systems, even when a high concentration of the sites (40%) are occupied by non-magnetic ions [22]. This finding raises natural questions about the versatility and robustness of magnetic order in HEOs more generally. In particular, are there limitations on the types of magnetically

ordered states that can be obtained in a high entropy material and how does magnetic dilution interface with the strong configurational disorder? In contrast to the much-studied rock salt HEO, in the spinel structure it becomes possible to synthesize a five-component material $(Cr,Mn,Fe,Co,Ni)_3O_4$ composed entirely of magnetic transition metals [23]. Previous studies on this material revealed long-range magnetic order [23–25] and remarkable electrochemical properties, raising interest in their potential for energy applications [26–32]. Additionally, spinels present the possibility for site selectivity stemming from competing enthalpy and crystal field effects, further enriching the complexity of their magnetic properties [33].

In this paper, we attempt to disentangle the effects of configurational disorder and magnetic dilution on the magnetic ground state of the spinel HEO $(Cr,Mn,Fe,Co,Ni)_3O_4$ as a function of non-magnetic Ga substitution. Gallium is the ideal candidate for magnetic dilution in this family, as in addition to carrying no magnetic moment, it is known to form ternary spinel phases with most of the ions present [34–37], and, further, its ionic radius is similar to that of the $3d$ transition metals and therefore produces negligible chemical pressure effects. We characterize the effect of this magnetic dilution through an ensemble of measurements with sensitivity to varying length scales (long and short-range order) and degrees of freedom (magnetic and structural). We find that long range ferrimagnetic order is robust across all Ga concentrations. However, the ordering temperature, magnetic hardness, and saturation moment all vary sensitively with composition, resulting in a highly tunable magnetic system. Locally, Ga-substitution enhances the configurational disorder of the spinel HEO system, with the more versatile ions (Mn, Fe, and Co) accommodating for charge imbalances. Spinels are therefore found to be an exemplary system to study the interactions between configurational disorder, magnetic dilution, and crystal field effects.

II. EXPERIMENTAL DETAILS

A. Solid-state synthesis

Polycrystalline samples of $(Cr,Mn,Fe,Co,Ni)_3O_4$ and its gallium substituted analogs (10%-Ga, 20%-Ga, and 40%-Ga) were synthesized by solid state reaction. Stoichiometric mixtures of MnO_2, Fe_2O_3, Cr_2O_3, Co_3O_4, NiO, and Ga_2O_3 were initially combined in a mortar and pestle, where they were ground by hand until visibly homogeneous. Next, the mixtures were mechanically homogenized for three hours in a ball mill using zirconia milling balls and ethanol to form a slurry. The mixed oxide powders were then dried in air and briefly reground in a mortar and pestle before being pressed into a pellet. The pressed pellets were placed into alumina crucibles and reacted in air by slow heating to 1050 °C over 11 hours and dwelling at this temperature for an additional 36 hours. The samples were thermally quenched by direct extraction from the furnace.

B. Powder x-ray diffraction & energy dispersive x-ray spectroscopy

Powder x-ray diffraction measurements were performed at room temperature on a Bruker D8 Advance Diffractometer with a copper source and a Johansson monochromator giving a monochromatic beam of wavelength $\lambda_{K_{\alpha 1}} = 1.5406$ Å. This system is equipped with a LYNXEYE XE-T silicon strip detector which is able to efficiently filter background fluorescence, which is significant for the elements involved. Measurements were performed over $10 \leq 2\theta \leq 80$ with a step of size of $0.019°$ 2θ. Rietveld refinements were performed with FullProf [38]. Energy dispersive x-ray spectroscopy (EDX) measurements were performed on a Philips XL30 scanning electron microscope equipped with a Bruker Quantax 200 energy-dispersion x-ray microanalysis system and an XFlash 6010 SDD detector.

C. Magnetic susceptibility

Temperature and field dependent magnetic susceptibility measurements were performed using a Quantum Design MPMS3 SQUID magnetometer. Samples were mounted in gel capsules and susceptibility measurements were performed under field-cooled and zero field-cooled protocols at temperatures between 2 and 400 K in a field of $H = 0.01$ T. For only the 0% Ga sample, in order to reach the paramagnetic state, measurements were extended to 600 K using the Oven option. Magnetization isotherms were collected at $T = 2$, 100, 200, 300, and 400 K for each sample for fields between -7 and 7 T. For each temperature, the sample was heated above its magnetic ordering transition and cooled under zero-field conditions before a full hysteresis loop was measured.

D. Neutron diffraction

Neutron diffraction measurements were carried out on the HB-2A Neutron Powder Diffractometer at Oak Ridge National Laboratory's High Flux Isotope Reactor. A 1 gram sample of $(Cr,Mn,Fe,Co,Ni)_3O_4$ and 2-grams of the 20%-Ga substituted sample were loaded into annular vanadium sample cans. Measurements were performed in a closed cycle refrigerator with heating capabilities, allowing measurements to be performed between 4 and 500 K. Full diffraction patterns at selected temperatures were collected with a wavelength of $\lambda = 2.41$ Å, which is obtained using a vertically focusing Ge-113 monochromator. The full temperature dependence of the magnetic ordering was probed by measuring the intensity of the (111) Bragg peak continuously on cooling. The magnetic

symmetry analysis was performed with SARAh [39] and Rietveld refinements were carried out using FullProf [38].

E. X-ray magnetic circular dichroism

X-ray magnetic circular dichroism (XMCD) is a subset of x-ray absorption spectroscopy (XAS), consisting of irradiating a sample with left and right-handed circularly polarized light, measuring the resulting absorption spectra, and taking their difference. For the circular dichroism to occur, time-reversal symmetry must be broken, as in a magnetic material. As a core-electron spectroscopy, XMCD is element-specific, and also inherits XAS's sensitivity to the measured ions' local environment. These two properties, combined with its magnetic sensitivity, make XMCD an ideal probe for systems with multiple magnetic ions.

The XAS and XMCD experiments were carried out at the REIXS beamline of the Canadian Light Source [40]. The sample temperature was 21K during the experiments, and the spectra were measured using an energy resolving silicon drift detector. Inverse partial fluorescence yield spectra were obtained by monitoring the oxygen fluorescence signal while scanning the transition metal $L_{2,3}$ edges. The measurements were then contrasted with ligand field multiplet theory calculations performed using the Crispy graphical user interface [41] to the Quanty code [42, 43]. Detailed descriptions and lists of parameters for the simulations are provided in the Supplemental Materials. Briefly, the parameters were adapted from existing references for Cr [44], Mn [45–47], Fe [48], Co [45, 49–51], and Ni [52]. Ga, having a fully filled 3d shell, cannot be measured in an XMCD experiment.

III. RESULTS AND DISCUSSION

A. Crystal structure

Polycrystalline samples of the spinel high entropy oxide $(Cr,Mn,Fe,Co,Ni)_3O_4$ and its gallium substituted analogs (10%-Ga, 20%-Ga, and 40%-Ga) were synthesized by solid state reaction. The spinel phase was initially confirmed by powder x-ray diffraction. Rietveld refinements of the 0% and 20% Ga samples are presented in Figure 1(a,b) showing excellent agreement with the cubic spinel phase (space group $Fd\bar{3}m$). Structural characterization for the 10% and 40% samples are available in the Supplemental Materials. The refined lattice parameters and adjustable oxygen coordinates as a function of Ga substitution are presented in Table I. The cubic spinel structure with the general formula AB_2O_4, as shown in Figure 1(c), has two distinct cation sublattices. The first, indicated in yellow is the tetrahedrally coordinated A-sublattice, while the second is the octahedrally coordinated B sublattice, indicated in blue. Independently, these A and B sublattices form, respectively, a diamond and pyrochlore network. From analogy with other known $3d$ transition metal based spinels, one may infer a strong site preference among the different cations but due to the similar atomic form factors of the elements involved, this cannot be resolved by x-ray diffraction. This site selectivity will be a major focus in the sections that follow.

Two minor impurity phases are evident in *only* the 0% Ga sample, which are zirconia and rock salt phases making up approximately 1% and 2% of the sample by volume, respectively. The zirconia phase originates from the degradation of the milling balls during the ball milling step of the reaction and is not of concern to the magnetic property measurements. The minor rock salt phase has all of its Bragg reflections sitting directly atop spinel main phase peaks and was only detected due to the extremely high resolution of our diffractometer. The refined lattice parameter for the rock salt impurity is in good agreement with that of NiO [53] and we therefore tentatively assign the likely origin of this phase as being due to Ni segregation, which we will further discuss later in the context of the local environment. Our preliminary investigations of this indicate that longer annealing times increase the fraction of the rock salt phase and this in-and-of-itself indicates that the spinel HEO cannot be considered as an entropy stabilized phase. Indeed, we speculate that minor rock salt impurities are likely common to other reported samples given their overlapping structure factors.

Energy dispersive x-ray spectroscopy (EDS) measurements, shown for the 0% and 20% Ga samples in Figure 1(d,e) were employed to investigate the composition and homogeneity of these samples on a microscopic length scale. The homogeneous distribution of Cr, Mn, Fe, Co, and Ni in both samples, and Ga in the 20% Ga sample, confirms the spacial homogeneity of the samples. The current results exclude any possible phase segregation on the length scale, micron scale, possible with SEM, and future measurements with a transmission electron microscope (TEM) can help us confirm the homogeneity on an even smaller length scale, nanometer scale. The current SEM-EDS mapping and the XRD results support the single phase nature of our s-HEO samples for different Ga doping levels.

B. Magnetic Susceptibility: Onset of ferrimagnetic order

We begin our magnetic characterization of the spinel HEO by considering the temperature dependent magnetic susceptibility for $(Cr,Mn,Fe,Co,Ni)_3O_4$, measured between 2 and 600 K, which is presented in Fig. 2(a). The onset of long-range magnetic order at $T_C = 403$ K [54] is marked by a sharp increase in the susceptibility and a bifurcation of the field-cooled and zero field-cooled susceptibilities, measured in an applied field of $H = 100$ Oe. While the low-field susceptibility data could be consistent with either ferro- or ferri-magnetic order, the latter is confirmed via isothermal magnetization measurements,

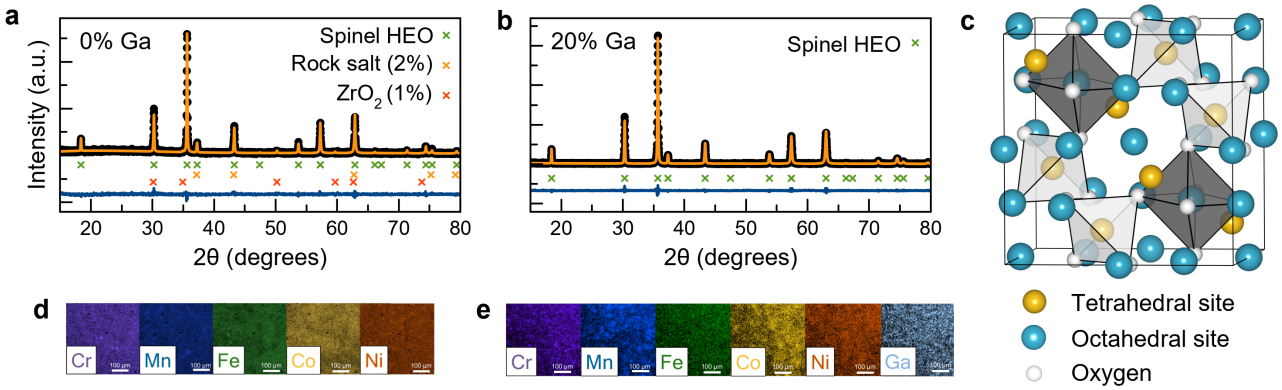

FIG. 1. Structural characterizations of the HEO spinels. Rietveld refinement (yellow lines) of the powder x-ray diffraction data (black circles) on the (**a**) 0% Ga and (**b**) 20% Ga samples confirm the cubic spinel phase (residual indicated by the blue line). The Bragg peak positions for the $Fd\bar{3}m$ spinel structure are indicated by the green crosses. Minor rock salt and zirconia impurities in the 0% sample are indicated by yellow and orange crosses, respectively. (**c**) The cubic spinel structure is made up of tetrahedrally coordinated (yellow) and octahedrally coordinated (blue) cation sites. Energy dispersive x-ray spectroscopy mapping for the (**d**) 0% and (**e**) 20% Ga samples reveal that the elemental distribution in these spinel HEOs are homogeneous on the micron scale.

presented in Fig. 2(b). At $T = 2$ K, the saturated magnetic moment reaches a value of $\mu_{\rm sat} = 1.52\ \mu_{\rm B}$ per formula unit (FU), which is smaller than even the smallest expected moment for any of the five magnetic transition metals involved and significantly smaller than the average expected moment. Therefore, we can conclude that the ordered moments on the A and B sublattices are aligned antiparallel and the saturated moment measured here represents the difference between the sublattice magnetizations ($\mu_{\rm sat} = |\mu^A_{\rm ord} - \mu^B_{\rm ord}|$). With the exception of the $T = 400$ K data set, which is above the ordering temperature, measurable but small hysteresis is detected at all other temperatures, with the coercive field reaching $H_c = 36$ mT at 2 K, characteristic of soft magnetic behavior. Finally, we note the appearance of a second feature in the zero field-cooled susceptibility at $T^* = 55$ K, which is more evident when viewing the derivative with respect to temperature, plotted in the top panel of Fig. 2(a). As this feature online appears in the zero field-cooled data, we tentatively assign it as a depinning transition, where thermal effects overcome disordering allowing some domains to spontaneously realign towards the applied field. Our magnetometry results on $(Cr,Mn,Fe,Co,Ni)_3O_4$ are in good agreement with previous reports [33, 55, 56].

The field-cooled magnetic susceptibility for $(Cr,Mn,Fe,Co,Ni)_3O_4$ and each of the Ga-substituted samples is presented in Fig. 2(c) and zero field-cooled data are available in the Supporting Information. The susceptibility data show that the onset of long-range magnetic order is suppressed continuously by magnetic dilution via substitution of non-magnetic Ga, reaching $T_C = 121$ K for the 40%-Ga sample. Meanwhile the T^* depinning transition temperature is found to increase with Ga-concentration (see derivative plots in the Supporting Information), consistent with increasing magnetic disorder, and is altogether absent in the 40%-Ga sample, apparently coinciding with T_C. The evolution of T_C and T^* is presented in Fig. 2(e), showing that T_C decreases approximately linearly with Ga-concentration. Extrapolating this trend towards $T_C = 0$ gives a critical Ga concentration of 58%, which would correspond to a percolation threshold of $x_p = 0.42$. This value can be approximately contrasted with the numerical result for ordered spinels, AB_2O_4, where both A and B are magnetic, which is $x_p = 0.227(3)$ when both sublattices are randomly diluted and $x_p = 0.071(2)$ or $x_p = 0.092(2)$ when the dilution selectively occurs on the A or B sublattice, respectively [57]. Thus, disorder effects in the spinel HEO appear to significantly enhance the suppression of magnetic order, despite the robustness of the magnetic order in the 0% compound.

Magnetization isotherms collected at $T = 2$ K for each sample are shown in Fig. 2(d) while higher temperatures are shown in the Supporting Information. Naively, one might expect the replacement of magnetic transition metals with non-magnetic Ga to yield a monotonic decrease in the net moment, which is not borne out by the data. Instead, the saturated moment, when normalized per formula unit, jumps from $\mu_{\rm sat} = 1.52\ \mu_{\rm B}$/FU in the 0% Ga sample to over 2 $\mu_{\rm B}$/FU for both 10% and 20% Ga. Only at 40% Ga does the saturated moment finally drop below the 0% value. Normalizing the same data per magnetic transition metal, as shown in Fig. 2(f), shows a similar trend with the exception of the 40% sample, which has $\mu_{\rm sat} = 0.68\ \mu_{\rm B}$/TM that exceeds the 0% sample. There are two possible contributing factors to these observations: (i) the non-magnetic Ga selectively occupies one of the sublattices yielding a larger difference between the sublattice ordered moments ($\mu_{\rm sat} = |\mu^A_{\rm ord} - \mu^B_{\rm ord}|$) and (ii) in order to satisfy charge neutrality, Ga-substitution induces a change of valence for one or more of the cations from 3+ towards 2+, increasing the average moment per transition

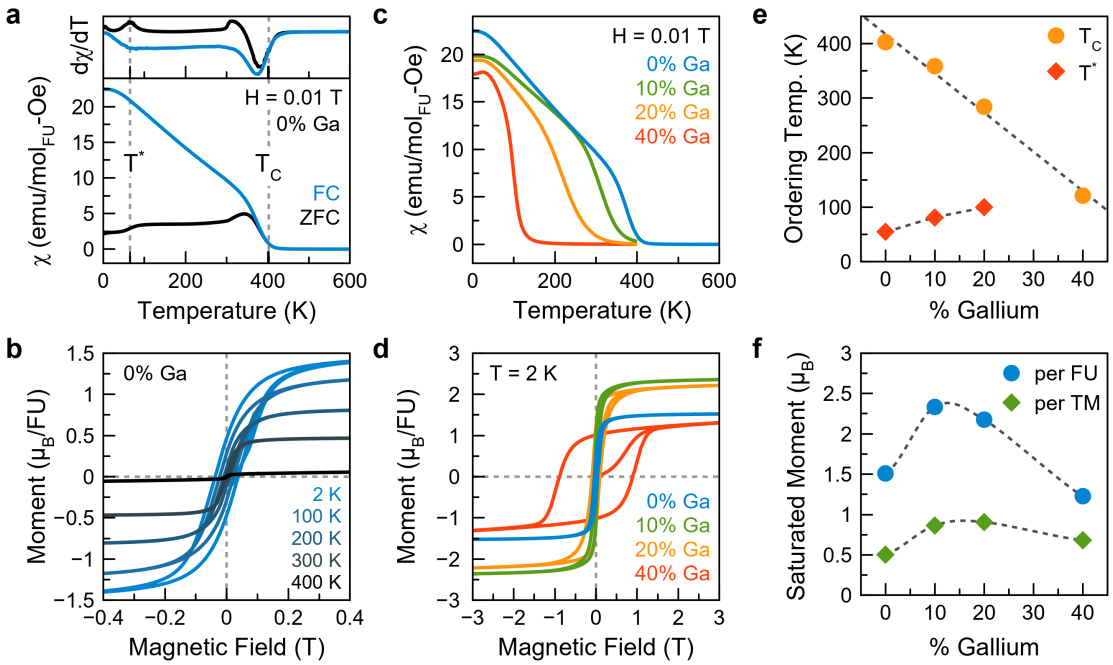

FIG. 2. Summary of magnetic property measurements performed on the the HEO spinels. (**a**) Magnetic susceptibility and (**b**) magnetization of $(Cr,Mn,Fe,Co,Ni)_3O_4$ revealing the onset of ferrimagnetic order at $T_C = 403$ K followed by a second anomaly at $T^* = 55$ K and a small hysteresis within the ordered state with a saturated moment of 1.52 μ_B per formula unit (FU). (**c**) The field-cooled magnetic susceptibility and (**d**) $T = 2$ K magnetization for the Ga-substituted HEO-spinels showing the suppression of magnetic order and a widening hysteresis with increasing Ga-concentration. The variation of (**e**) T_C and T^* and (**f**) the saturated moment per formula unit and per magnetic transition metal (TM) with Ga-concentration.

metal. Magnetometry data alone do not provide enough information to disentangle these two effects and we will return to both of these points in the section on neutron diffraction and x-ray absorption spectroscopy that follow.

The $T = 2$ K magnetization isotherms also exhibit a pronounced magnetic hardening as a function of Ga concentration. There is a moderate increase in the coercive field going from 0% to 20% and a dramatic increase at 40% Ga, where $H_c = 880$ mT. This effect can be partially attributed to increasing magnetic disorder. However, change of valence for individual transition metals may also be a culprit and we will return to this point as well.

C. Neutron diffraction: Magnetic structure determination

To complete our characterization of the magnetically ordered state in the spinel HEO, we performed powder neutron diffraction measurements on the 0% and 20% Ga-substituted samples. There has been one previous neutron diffraction measurement on $(Cr,Mn,Fe,Co,Ni)_3O_4$ [33]; however, this study only includes only a single data set, collected at $T = 300$ K, which does not allow the nuclear and magnetic structures to be separately determined, nor does it represent the magnetic ground state since the magnetism continues to evolve considerably below 300 K, as shown by the magnetic susceptibility data in Fig. 2(a). In our experiment, we performed measurements between $T = 4$ and 500 K, giving us access to both the paramagnetic regime as well as within the ordered state.

Starting with first the 0% Ga sample, upon cooling through the ordering transition at $T_C = 403$ K, we observe the formation of intense magnetic Bragg peaks that sit atop the nuclear Bragg peaks, as can be seen by viewing the intensity of (111) Bragg peak as a function of temperature shown in Fig. 3(a). The onset of this magnetic order agrees well with the transition temperature detected from susceptibility and we can see that the order moment continues to grow monotonically with decreasing temperature before finally saturating at close to 50 K. Comparing the (111) Bragg peak at 500 K, where it is purely nuclear in origin, and 4 K, where it is overwhelmingly magnetic in origin, we can see that there is no significant difference in the line width, indicating that within the resolution limit of this diffractometer, the magnetic order is truly long-range in nature. We can estimate the minimum correlation length by considering the full-width and half maximum of the (111) Bragg peak and this gives $\xi = {}^{2\pi}/_{\text{FWHM}} = 294(2)$ Å.

In order to determine the nature of the magnetically ordered state, we perform a Rietveld analysis of the full diffraction pattern, as shown in Figure 3(b)). Above the onset of magnetic order, at $T = 500$ K, our refinement shown in the top panel includes three phases: (i) the cubic spinel structure with space group $Fd\bar{3}m$, (ii)

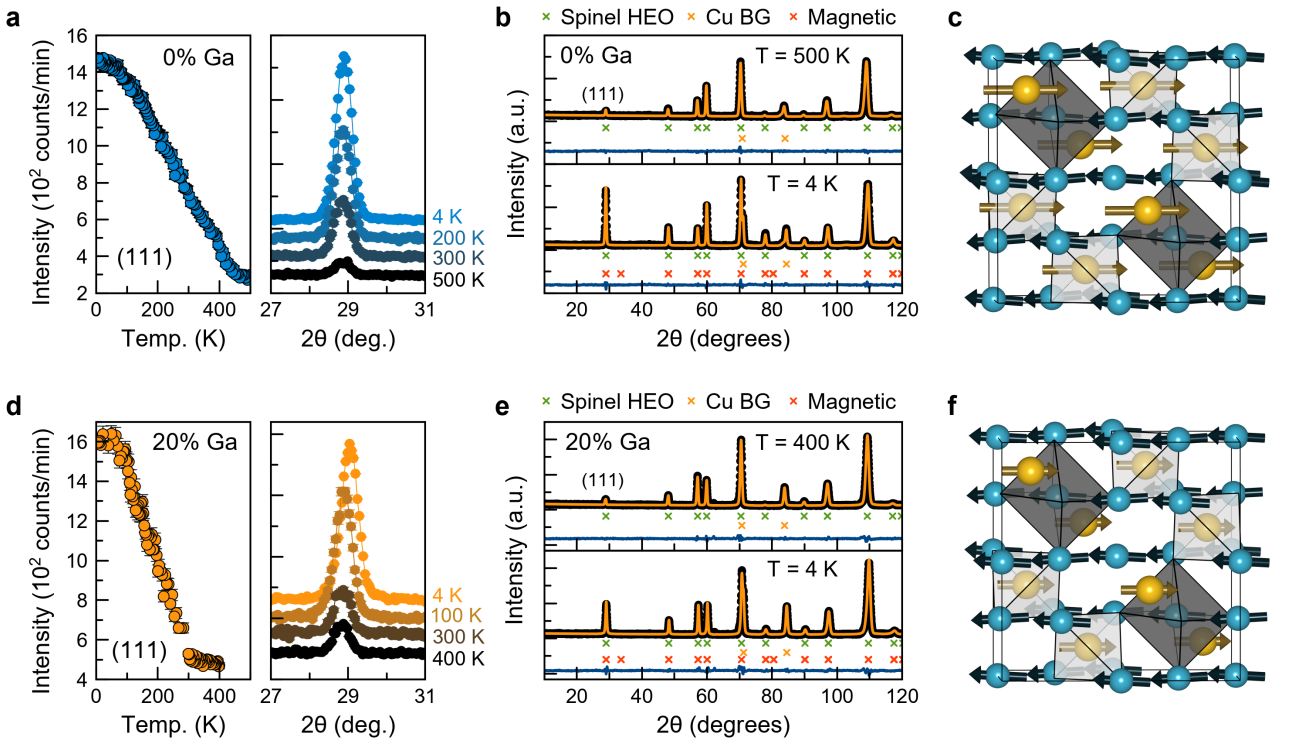

FIG. 3. Neutron diffraction measurements and magnetic structure determination for the HEO spinels. The top set of panels show data for the 0% Ga sample and the bottom set of panels are for the 20% Ga sample. (**a,d**) The temperature dependence of the (111) Bragg peak peak shows a sharp increase indicating the onset of $k = 0$ magnetic order. (**b,e**) Rietveld refinements in the paramagnetic ($T = 500$ K for the 0% Ga sample and $T = 400$ K for the 20% Ga sample) and magnetically ordered ($T = 4$ K) states allow the determination of the magnetic structure. Tick marks indicate the positions of Bragg peaks for the spinel nuclear structure (green), the copper background from the sample environment (yellow), and the $k = 0$ magnetic structure (orange). (**c,f**) Both the 0% Ga and 20%Ga samples exhibit the ferrimagnetic Γ_9 structure, in which the tetrahedral moments in yellow point exactly along the $\langle 100 \rangle$ while the octahedral moments in blue are slightly canted away from $\langle 100 \rangle$. Ga-substitution strongly suppresses the tetrahedral moment.

a metallic Cu phase, which originates from the sample environment, and (iii) minor ZrO_2 and NiO phases (as described previously in the x-ray diffraction section, tick marks for these phases are omitted for clarity). The coherent scattering lengths of our five transition metals span a large range, from -3.73 barns for Mn to 10.3 barns for Ni. One might therefore hope to be able to independently refine the site occupations from the neutron data. However, in our analysis, we found that due to tradeoffs with other refined parameters (such as the thermal parameters, B_{iso}, and the oxygen occupancy), we could not meaningful distinguish via their χ^2 values between a range of plausible cation distributions. Given that our primary goal is to refine the magnetic structure, we therefore constrained the number of adjustable parameters in our refinement of the nuclear structure by allowing only minor deviations from the cation distribution deduced from the XMCD analysis, which will be described in the section that follows, and fixed the oxygen occupancy at 100%. This yielded excellent agreement between the data and the model and physically reasonable values for all other refined parameters.

Upon cooling into the magnetically ordered state, we observe that all magnetic Bragg peaks are located at positions allowed by the face-centered cubic selection rules of the nuclear structure. Therefore, we can characterize the magnetic order as having a propagation vector of $k = 0$. We next consider the symmetry allowed magnetic structures for the tetrahedral and octahedral sites, which correspond to the $8a$ and $16d$ Wyckoff sites, respectively. Following the representation analysis formalism, we can define these symmetry allowed magnetic structures according to their irreducible representations (Γ composed of basis vectors ψ). There are two possible $k = 0$ states for the tetrahedral site, which are Γ_8 and Γ_9, while there are four possible states for the octahedral site: Γ_3, Γ_5, Γ_7, and Γ_9. In cases where there is a coupled ordering transition involving two sublattices simultaneously, it is required that both sites order in the same representation group. Thus, by symmetry arguments alone one can deduce that the ordering should involve the Γ_9 irreducible representations for both the A and B sublattice. However, this assessment can be validated through checking all linear combinations of the irreducible representations and indeed, only a state involving Γ_9 on both sublattices can give a satisfactory agreement with the data. The

TABLE I. Structural and magnetic properties of the Ga-substituted HEO spinels determined from x-ray diffraction (cubic lattice parameter a and adjustable oxygen coordinate), magnetic susceptibility (ordering temperature T_C and depinning transition T^*), magnetization (saturated moment per formula unit and per transition metal, and coercive field) and magnetic neutron diffraction (tetrahedral and octahedral sublattice moments for 0% and 20% samples only).

	a (Å)	O coord.	T_C (K)	T^* (K)	$\mu_{\rm sat}$/FU ($\mu_{\rm B}$)	$\mu_{\rm sat}$/TM ($\mu_{\rm B}$)	Coerc. (mT)	$\mu_{\rm tet}$ ($\mu_{\rm B}$)	$\mu_{\rm oct}$ ($\mu_{\rm B}$)
0% Ga	8.3539(3)	0.2558(5)	382	55	1.51	0.50	36	3.60(6)	2.5(1)
10% Ga	8.3375(2)	0.2580(3)	319	81	2.33	0.86	40	-	-
20% Ga	8.3397(2)	0.2569(3)	230	100	2.18	0.91	98	2.46(6)	2.49(9)
40% Ga	8.3542(2)	0.2566(3)	102	-	1.23	0.68	880	-	-

resulting refinement at $T = 4$ K is shown in the lower panel of Figure 3(b), which in addition to the Γ_9 magnetic structure contains the same set of structural phases as the $T = 500$ K refinement.

The spin configuration for the refined magnetic structure of the spinel HEO is shown in Figure 3(c). The Γ_9 representation for the tetrahedral site is a ferromagnetic arrangement composed of a single type of basis state (triply degenerate for cubic symmetry) in which the moments points exactly along the cubic ⟨100⟩ directions with an ordered moment of $\mu_{\rm tet}$ =3.60(6) $\mu_{\rm B}$, represented by the yellow sublattice in Fig. 3(c). The Γ_9 representation for the octahedral site is composed of two types of basis states (each triply degenerate for cubic symmetry) in which the moments point along non-coplanar ⟨111⟩ and ⟨211⟩ directions, respectively. Linear combinations of these two basis states can also produce a ferromagnetic arrangement with moments pointing along the cubic ⟨100⟩ directions with an ordered moment of $\mu_{\rm oct}$ =2.5(1) $\mu_{\rm B}$, as shown for the blue sublattice in Fig. 3(c). The two sublattices are aligned anti-parallel to one another, confirming the ferrimagnetic order deduced from our magnetization data. In our refinement, the best agreement with the experimental data occurred when the moments on the octahedral sites are canted by a small amount, $\alpha = 6.1$ degrees from the ⟨100⟩ direction. Such canting is well known for ferrimagnetic spinels and is often referred to as the Yafet-Kittel angle [58, 59]. Detailed characterizations of many spinel solid solutions has shown that the magnitude of this canting is highly correlated with the specific pairwise interactions between the tetrahedral (A) and octahedral (B) sublattices, which in turn depends strongly on the specific composition and the degree of inversion and magnetic dilution [60]. The presence of canting indicates a certain degree of competition between inter- (J_{AB}) and intra- (J_{AA} and J_{BB}) sublattice exchange interactions, with a strong, antiferromagnetic J_{BB} disrupting the antiferromagnetic coupling between the A and B sublattices. The refined net moment is $\mu_{\rm net}$ =1.4(2) $\mu_{\rm B}$ per formula unit, in excellent agreement with the saturated moment observed in magnetization.

For the 20% Ga substituted sample, we see similar behavior with a sharp increase in the intensity of the (111) Bragg peak that correlates well with $T_C = 284$ K detected by magnetic susceptibility (Fig. 3(d)). Interestingly, by comparing panel (a) and (d) of Fig. 3, one can see that while there is no perceptible shift in the position of the (111) peak in the 0% sample with temperature, corresponding to negligible thermal effects on the lattice parameter, one can see that between 100 K and 4 K, there is a rather significant shift to higher angles in the 20% Ga sample, corresponding to a contraction of the lattice. It is somewhat unusual that the thermal effects on the lattice should be so pronounced in this temperature range and may herald some coupling between magnetic and lattice degrees of freedom.

Similar to our protocol in the 0% Ga case, in our Rietveld refinement of the 20% Ga sample we allow only small deviations from the cation distribution deduced from the XMCD analysis to be shown in the next section. The resulting refinement of the structure in the paramagnetic state at $T = 400$ K gives excellent agreement with the data as shown in Fig. 3(e). The refinement in the magnetically ordered state, at $T = 4$ K confirms that the magnetic order is described by the same Γ_9 ferrimagnetic state observed in the 0% sample, with an unchanged B sublattice ordered moment of $\mu_{\rm oct}$ =2.49(9) $\mu_{\rm B}$ but a substantially reduced A site ordered moment of $\mu_{\rm tet}$ =2.46(6) $\mu_{\rm B}$, which is approximately two-thirds the value obtained for the 0% Ga sample. This supports our previous claim that non-magnetic gallium is preferentially occupying the tetrahedral site. An additional consequence of the highly suppressed A sublattice moment, is that there is a less complete cancellation between the antiparellel A and B sublattice moments such that the net moment increases to $\mu_{\rm net}$ =2.5(2) $\mu_{\rm B}$, as compared to $\mu_{\rm net}$ =1.4(2) $\mu_{\rm B}$ in the 0% sample. This also accounts for the observed increase in the saturated moment found in magnetization measurements. Finally, the refined canting angle for the octahedral moments in the 20% Ga sample, $\alpha = 4.6$ degrees, is reduced from the 0% case, consistent with reduced competition between inter- and intra-sublattice exchange interactions.

D. XAS and XMCD: Local ordering and site selectivity

X-ray magnetic circular dichroism (XMCD) is one of the select few pathways to determining site occupancies in transition-metal spinel oxides [61] due to its simultaneous chemical and crystal field sensitivity. Site occupancies can

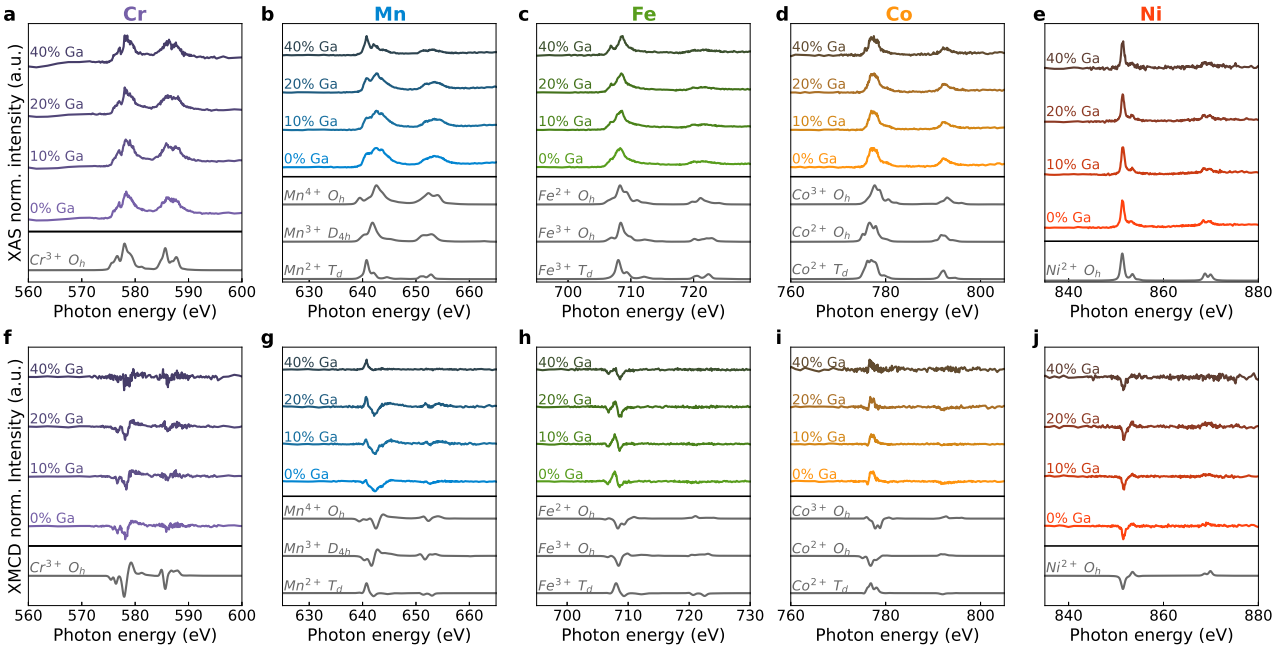

FIG. 4. Normalized x-ray magnetic circular dichroism (XMCD) data and multiplet calculations from measurements performed on the HEO spinel samples with varying Ga concentration at the transition metal $L_{2,3}$ edges. Top row: L+R spectra for (**a**) Cr, (**b**) Mn, (**c**) Fe, (**d**) Co, and (**e**) Ni. The coordination environment can be deduced from these signals, which are approximately equivalent to pure x-ray absorption spectroscopy (XAS) measurements. Bottom row: L-R (XMCD) spectra for (**f**) Cr, (**g**) Mn, (**h**) Fe, (**i**) Co, and (**j**) Ni. The sign of each spectrum reflects the ferrimagnetic arrangement in the HEO spinels. Predominantly positive signals correspond to mainly tetrahedral states (T_d) while negative signals indicate a mostly octahedral coordination (O_h).

be deduced by comparison with multiplet calculations, which depend on both the coordination and the valence of the transition metal in question. XMCD measurements for the spinel HEO samples, along with the corresponding multiplet calculations, are presented in Fig. 4, where the top row of panels are the sum of the left and right circularly polarized responses (L+R) and therefore correspond approximately to x-ray absorption spectroscopy (XAS) while the bottom row is the difference (L-R), corresponding to the dichroism. The spectra are presented normalized to their maxima, so the main features can be resolved across the entire composition range. An important feature of these spectra is that, for ferrimagnetic spinels, one can observe the antiferromagnetic coupling of the tetrahedral and octahedral sites in a straightforward manner. The sign of the XMCD signal is directly dependent on the number of available holes in the transition metal ions' *d*-shell and since the holes for the octahedral and tetrahedral sites have opposing spin, the XMCD will have opposite sign. While it is not possible to directly measure the site occupancy of Ga in this way due to its filled *d*-shell, its distribution can be approximately deduced from the constraint that the stoichiometry respects the spinel structure.

The analysis of Cr and Ni from Fig. 4(a,f) and (e,j) is straightforward as neither are observed to change as a function of Ga concentration. Both are found exclusively in an octahedral (O_h) coordination, as indicated by the negative dichroism with Cr in a 3+ oxidation state and Ni in a 2+ oxidation state. In both cases, the multiplet calculation describes well all the features in both the absorption and the dichroism spectra. The remaining cations will be discussed in order of increasing complexity.

A small shoulder-like feature in the XAS spectrum appears when a 40% Ga concentration is reached. This observation can be explained by the presence of Co^{2+} in octahedral coordination, which also elucidates the origin of the increased coercivity observed in Fig. 2(d). Upon closer inspection of the spectra corresponding to 10% and 20% Ga-diluted samples, the emergence of these features can already be observed, albeit on a smaller scale. While more subtle than the effect it has on other ions, this change is then identified as a direct consequence of Ga substitution. As seen in Fig. 4(c), Fe is in an admixture of states in all samples, requiring a more nuanced analysis. Here, we start by considering the most extreme case. At 40% Ga substitution, a sharp feature can be observed at around 707 eV, which aligns well with the multiplet calculation for Fe^{3+} in octahedral coordination. While it appears to be the main contribution, the corresponding XMCD signal from Fig. 4(h) indicates that it is not the only one, as there is an additional, positive, contribution that is absent in the Fe^{3+} octahedral state. The positive XMCD signal is instead consistent with Fe^{3+} in tetrahe-

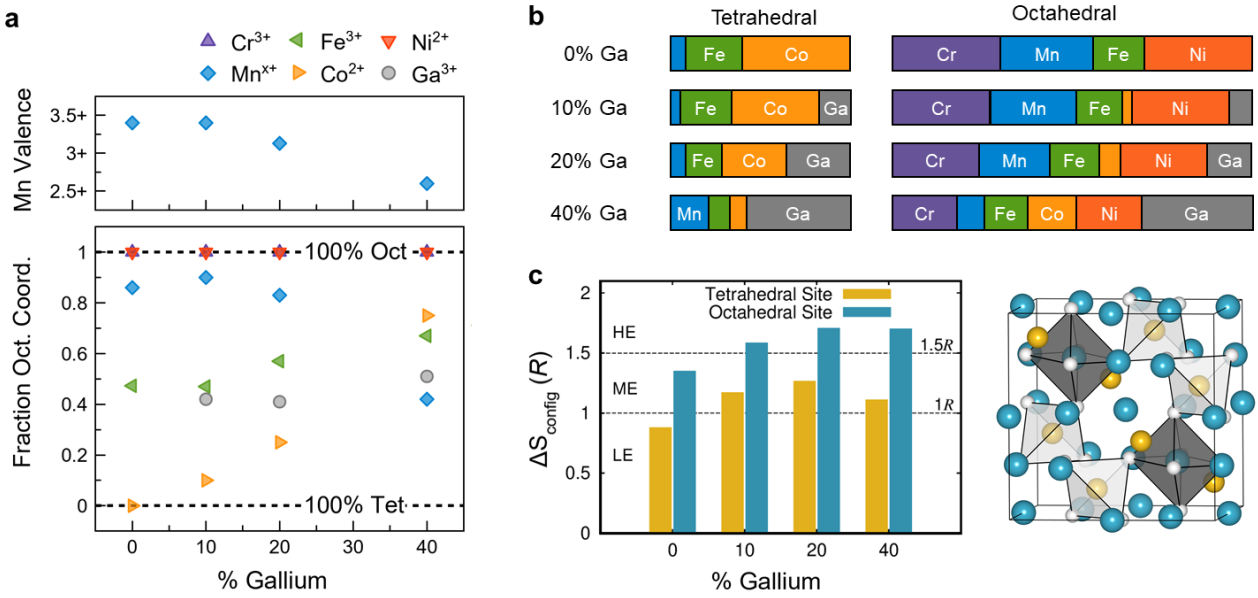

FIG. 5. Summary of cation distributions and sublattice entropies in the spinel HEO as a function of Ga substitution. (**a**) The valence of Mn and the fraction of octahedral occupation as a function of Ga concentration. Preferential occupation of Ga onto tetrahedral sites causes a shift of Fe and Co towards the octahedral site and the stable 3+ valence of Ga is compensated by a reduction in the valence of Mn, which in its 2+ valence state prefers tetrahedral sites. (**b**) Schematic representation of the cation occupation of the tetrahedral and octahedral sites for each sample. (**c**) Calculated sublattice entropy as a function of Ga concentration for the tetrahedral site in yellow and the octahedral site in blue. At 0% Ga, neither sublattice surpasses the empirical threshold for high entropy but with Ga substitution high and medium entropy is achieved for the octahedral and tetrahedral sites, respectively.

dral coordination. With decreasing Ga concentration, the shoulder in the XAS recedes and the XMCD becomes mainly positive. We therefore conclude that Fe remains in a 3+ oxidation state across the analyzed composition range and gradually shifts from mainly tetrahedral at 0% towards a primarily octahedral state around 20% Ga substitution.

The final ion to consider is Mn, whose behavior is the most challenging to explain and reproduce with multiple calculations, particularly for the low Ga-concentration samples. From Fig. 4(b), we observe three broad features centered around 640 eV in the L_3 edge at lower Ga substitution, which are replaced by two comparatively sharp features at 40% Ga concentration. The features in the 40% sample are well explained by the spectrum for Mn^{2+} in tetrahedral coordination, which is corroborated by inspection of the XMCD signal in Fig. 4(g). As a function of decreasing Ga concentration, the Mn^{2+} tetrahedral signal persists but becomes weaker as simultaneously the XMCD becomes increasingly negative. At 0% the most prominent signal is located at 640.7 eV and this feature is attributed to Mn^{3+} in a tetragonally distorted octahedron (D_{4h} symmetry) due to a strong Jahn-Teller effect. The final feature in the L_3 edge is located at 641.9 eV, and corresponds to the presence of Mn^{4+} in octahedral coordination, whose presence can be traced back to the use of MnO_2 as the Mn reagent in the synthesis procedure.

The evolution of Mn in the sample can therefore be characterized as follows: the undiluted sample is characterized by the presence of all three Mn species, 2+ tetrahedral, 3+ tetragonally distorted octahedral, and 4+ octahedral. Upon the introduction of Ga to the structure, Mn accommodates the extra charge by gradually shifting towards the Mn^{2+} state in tetrahedral coordination. At 20% Ga, the Mn^{4+} octahedral signal has been reduced substantially, and by 40% Ga, Mn is predominantly in a 2+ tetrahedral state, with minimal 3+ D_{4h} and 4+ octahedral contributions.

Putting the analysis of all XMCD results together allows us to arrive at approximate site distributions and compositions for each of our four samples, as summarized in Fig. 5(a,b). We can see that the undiluted 0% Ga sample presents a significant degree of site selectivity, with Cr and Ni exclusively occupying octahedral sites, Co only in tetrahedral sites, and mixed occupations for Mn and Fe, leading to the estimated composition for the tetrahedral site of $A = Mn^{2+}_{0.08}Fe^{3+}_{0.32}Co^{2+}_{0.6}$ and for the octahedral site of $B = Cr^{3+}_{0.6}Mn^{3+}_{0.2}Mn^{4+}_{0.32}Fe^{3+}_{0.28}Ni^{2+}_{0.6}$. The result for the 0% Ga sample can be compared with the previous study by Sarkar *et al.*, where it was concluded that Co was present in an almost equal mixture of 3+ and 2+ tetrahedral states, while Mn was ascribed as being almost entirely 3+ octahedral with a minor 2+ octahedral component [33]. One factor that might account for some of these differences is that the data collected in Ref. [33] used a total electron yield method, which is more surface

sensitive as compared to the inverse partial fluorescence yield method used here. Another intriguing possibility is that the fundamental differences between the results could be indicative of some dependence of the site selectivity on the synthesis method or thermal treatments performed on the samples.

Upon the introduction of Ga into the HEO spinel, the compositions of each sample can be qualitatively estimated from the XMCD spectra, with the distribution of Ga ions in each sample constrained so that the final composition respects the stoichiometry of the spinel structure. While Ga is divided almost evenly between the tetrahedral and octahedral sites (Fig. 5(a)), due to the 1:2 sublattice ratio in the spinel structure a larger fraction of the tetrahedral magnetic ions are replaced. Therefore, We find a preferential dilution of the tetrahedral sublattice, as shown schematically in Fig. 5(b), consistent with the trends observed in our magnetization data. Meanwhile, Co and Fe accommodate by gradually shifting to primarily octahedral crystal field environments (Fig. 5(a)). On the other hand, Mn seems to adapt to the additional charge (Ga's 3+ oxidation state is larger than the 2.667+ average for the spinel structure) by reducing towards a 2+ oxidation state, as shown in the upper panel of Fig. 5(a). At 20% Ga substitution, we find that the tetrahedral site has been 35% diluted by non-magnetic Ga while the octahedral site has only been diluted by just over 10%, consistent with the large reduction in the tetrahedral moment observed in our neutron diffraction analysis. The negligible change in the the octahedral sublattice moment can be ascribed to the larger fraction of high spin Mn^{3+} as compared to Mn^{4+} at this composition. By 40% Ga, the ion distribution reaches the estimated composition for the tetrahedral site of $A = Mn^{2+}_{0.21}Fe^{3+}_{0.12}Co^{2+}_{0.09}Ga^{3+}_{0.58}$ and for the octahedral site of $B = Cr^{3+}_{0.36}Mn^{3+}_{0.09}Mn^{4+}_{0.06}Fe^{3+}_{0.24}Co^{2+}_{0.27}Ni^{2+}_{0.36}Ga^{3+}_{0.62}$. Here we can see that non-magnetic Ga occupies more than 50% of the tetrahedral sites while only occupying approximately 25% of the octahedral sites.

E. Entropy analysis

With these results in mind, we can begin to construct a realistic estimate of the configurational entropy for each of these spinel HEOs taking into account the preferential occupation of multiple cation sublattices. Our deduced compositions, which are shown schematically in Fig. 5(b) respect the stoichiometry of the spinel structure and also obey charge neutrality with the oxygen sublattice within negligible error. Our assessment of the transition metal ion sites and valences agree with both the experimental XMCD spectra and also align well with the well-established crystal field behaviors for these ions. From this estimate, one can then compute the corresponding configurational entropy,

$$S_{\text{config}} = -R \sum_{ions} x \ln x \qquad (1)$$

where x is the fractional occupation of each ion inhabiting the site. Empirically it has been established that the threshold for medium entropy occurs at $S_{\text{config}} > 1R$ and high entropy occurs at $S_{\text{config}} > 1.5R$ where the conventional 5-component equiatomic high entropy oxide has $S_{\text{config}} = 1.61R$. The computed configurational entropy for each of our HEO spinels, separated by sublattice, is plotted in Fig. 5(c).

One can deduce on general grounds that site selecitivity in the spinel structure is a force that will act to reduce configurational entropy. Indeed in the 0% Ga case we find that the tetrahedral site, which is majority occupied by Co, falls in the low-entropy regime with $S_{\text{config,tet}} = 0.9R$, while the octahedral site has medium-entropy $S_{\text{config,oct}} = 1.35R$. However, if we consider the two different valences of Mn as contributing to the configurational entropy, this alone further enhances the octahedral to the high-entropy limit with $S_{\text{config,oct}} = 1.52R$. Likewise, the introduction of Ga as a 6th cation has an overall enhancing effect on the configurational entropy, with the tetrahedral site being elevated to medium-entropy and the octahedral site being raised to the high-entropy limit by 10% Ga. The maximum combined configurational entropy, among compositions we've studied is reached for the 20% Ga sample, which exceeds $S_{\text{config,total}} = 3R$. This finding implies that, with appropriate cation choice, the configurational entropy of the two sublattices of the spinel structure can likely be independently tuned and precisely controlled across different entropy regimes, which we term "entropy engineering".

IV. CONCLUSIONS

In this work, we have demonstrated that due to intense site selectivity, the magnetic ground state of the spinel HEO can be strongly tuned by non-magnetic Ga substitution. Magnetic susceptibility measurements show that the suppression in the onset of long-range magnetic order occurs significantly faster than one might expect from conventional percolation theory, suggesting that configurational disorder may be playing a prominent role. Simultaneously, there is a significant enhancement in the coercive field and a non-monotonic variation in the saturated moments.Our neutron diffraction measurements show that the ferrimagnetic order is robust in response to Ga-substitution, with a rapidly suppressed tetrahedral moment and a reduced inter sublattice frustration. Finally, our XMCD measurements reveal that the inclusion of Ga is accommodated through valence and site re-organizations for Mn, Fe, and Co, while Ni and Cr are unaffected. An extremely high entropy system with $S_{\text{config,total}} > 3R$ is realized for the 20% Ga sample and we show that the individual sublattice entropies can be precisely engineered by the choice of cations. We also demonstrate that multiple valences are a route to further enhancing the configurational entropy.

In light of these findings, many new avenues of in-

quiry beckon. For instance, are there any subsets of these five magnetic transition metals or different stoichiometries that would yield a non-ferrimagnetic ordered state? What is the fate of the ferrimagnetic order at higher nonmagnetic dilutions? Exploring the limit in which long-range magnetic order is completely suppressed will allow a more rigorous comparison with percolation theory. Along a different axis, the spectral XMCD differences between our work and Sarkar *et al.* [33] suggest that their may be significant sample dependence related to synthesis procedure and this topic remains largely unexplored. A better understanding of the exact level of configurational entropy in the spinel HEO is also, for now, out of reach. While our study suggests a very high level of site selectivity, there may be additional preferred short range configurations that will require highly sophisticated studies of ions in a pairwise fashion. We therefore conclude on the optimistic note that the field of high entropy oxides is still in its infancy and many important discoveries remain to be made.

ACKNOWLEDGMENTS

The authors thank Joerg Rottler and Solveig Stubmo Aamlid for insightful conversations on high entropy oxides. This work was supported by the the Natural Sciences and Engineering Research Council of Canada and the CIFAR Azrieli Global Scholars program. This research was undertaken thanks in part to funding from the Canada First Research Excellence Fund, Quantum Materials and Future Technologies Program.

[1] Christina M Rost, Edward Sachet, Trent Borman, Ali Moballegh, Elizabeth C Dickey, Dong Hou, Jacob L Jones, Stefano Curtarolo, and Jon-Paul Maria, "Entropy-stabilized oxides," Nature communications **6**, 1–8 (2015).

[2] Rui-Zhi Zhang and Michael J Reece, "Review of high entropy ceramics: design, synthesis, structure and properties," Journal of Materials Chemistry A **7**, 22148–22162 (2019).

[3] Corey Oses, Cormac Toher, and Stefano Curtarolo, "High-entropy ceramics," Nature Reviews Materials **5**, 295–309 (2020).

[4] Brianna L Musicó, Dustin Gilbert, Thomas Zac Ward, Katharine Page, Easo George, Jiaqiang Yan, David Mandrus, and Veerle Keppens, "The emergent field of high entropy oxides: Design, prospects, challenges, and opportunities for tailoring material properties," APL Materials **8**, 040912 (2020).

[5] Abhishek Sarkar, Ben Breitung, and Horst Hahn, "High entropy oxides: The role of entropy, enthalpy and synergy," Scripta Materialia **187**, 43–48 (2020).

[6] Scott J McCormack and Alexandra Navrotsky, "Thermodynamics of high entropy oxides," Acta Materialia **202**, 1–21 (2021).

[7] D Bérardan, S Franger, AK Meena, and N Dragoe, "Room temperature lithium superionic conductivity in high entropy oxides," Journal of Materials Chemistry A **4**, 9536–9541 (2016).

[8] Abhishek Sarkar, Leonardo Velasco, Di Wang, Qingsong Wang, Gopichand Talasila, Lea de Biasi, Christian Kübel, Torsten Brezesinski, Subramshu S Bhattacharya, Horst Hahn, *et al.*, "High entropy oxides for reversible energy storage," Nature communications **9**, 1–9 (2018).

[9] Abhishek Sarkar, Qingsong Wang, Alexander Schiele, Mohammed Reda Chellali, Subramshu S Bhattacharya, Di Wang, Torsten Brezesinski, Horst Hahn, Leonardo Velasco, and Ben Breitung, "High-entropy oxides: fundamental aspects and electrochemical properties," Advanced Materials **31**, 1806236 (2019).

[10] Yifan Sun and Sheng Dai, "High-entropy materials for catalysis: A new frontier," Science Advances **7**, eabg1600 (2021).

[11] Kurt E Sickafus, John M Wills, and Norman W Grimes, "Structure of spinel," Journal of the American Ceramic Society **82**, 3279–3292 (1999).

[12] Qing Zhao, Zhenhua Yan, Chengcheng Chen, and Jun Chen, "Spinels: controlled preparation, oxygen reduction/evolution reaction application, and beyond," Chemical reviews **117**, 10121–10211 (2017).

[13] EJW Verwey and EL Heilmann, "Physical properties and cation arrangement of oxides with spinel structures i. cation arrangement in spinels," The Journal of Chemical Physics **15**, 174–180 (1947).

[14] Hugh St C O'Neill and Alexandra Navrotsky, "Simple spinels: crystallographic parameters, cation radii, lattice energies, and cation distribution," American Mineralogist **68**, 181–194 (1983).

[15] Jie Song, Dong Wook Shin, Yuhao Lu, Charles D Amos, Arumugam Manthiram, and John B Goodenough, "Role of oxygen vacancies on the performance of Li[$Ni_{0.5-x}Mn_{1.5+x}$] O_4 ($x = 0$, 0.05, and 0.08) spinel cathodes for lithium-ion batteries," Chemistry of Materials **24**, 3101–3109 (2012).

[16] CE Rodríguez Torres, Gustavo Alberto Pasquevich, P Mendoza Zélis, Federico Golmar, SP Heluani, Sanjeev K Nayak, Waheed A Adeagbo, Wolfram Hergert, Martin Hoffmann, Arthur Ernst, *et al.*, "Oxygen-vacancy-induced local ferromagnetism as a driving mechanism in enhancing the magnetic response of ferrites," Physical Review B **89**, 104411 (2014).

[17] Eric C O'Quinn, Jacob Shamblin, Brandon Perlov, Rodney C Ewing, Joerg Neuefeind, Mikhail Feygenson, Igor Gussev, and Maik Lang, "Inversion in $Mg_{1-x}Ni_xAl_2O_4$ spinel: New insight into local structure," Journal of the American Chemical Society **139**, 10395–10402 (2017).

[18] Jue Liu, Xuelong Wang, Olaf J Borkiewicz, Enyuan Hu, Rui-Juan Xiao, Liquan Chen, and Katharine Page, "Unified view of the local cation-ordered state in inverse spinel oxides," Inorganic Chemistry **58**, 14389–14402 (2019).

[19] Alexandra Navrotsky and OJ Kleppa, "The thermodynamics of cation distributions in simple spinels," Journal of Inorganic and nuclear Chemistry **29**, 2701–2714 (1967).

[20] A Navrotsky and OJ Kleppa, "Thermodynamics of formation of simple spinels," Journal of Inorganic and Nuclear Chemistry **30**, 479–498 (1968).

[21] A Navrotsky, "Thermodynamics of A_3O_4-B_3O_4 spinel solid solutions," Journal of Inorganic and Nuclear Chemistry **31**, 59–72 (1969).

[22] Junjie Zhang, Jiaqiang Yan, Stuart Calder, Qiang Zheng, Michael A. McGuire, Douglas L. Abernathy, Yang Ren, Saul H. Lapidus, Katharine Page, Hong Zheng, John W. Freeland, John D. Budai, and Raphael P. Hermann, "Long-range antiferromagnetic order in a rocksalt high entropy oxide," Chemistry of Materials **31**, 3705–3711 (2019).

[23] Juliusz Dąbrowa, Mirosław Stygar, Andrzej Mikuła, Arkadiusz Knapik, Krzysztof Mroczka, Waldemar Tejchman, Marek Danielewski, and Manfred Martin, "Synthesis and microstructure of the (co,cr,fe,mn,ni)3o4 high entropy oxide characterized by spinel structure," Materials Letters **216**, 32–36 (2018).

[24] J. Cieslak, M. Reissner, K. Berent, J. Dabrowa, M. Stygar, M. Mozdzierz, and M. Zajusz, "Magnetic properties and ionic distribution in high entropy spinels studied by mössbauer and ab initio methods," Acta Materialia **206**, 116600 (2021).

[25] Aiqin Mao, Feng Quan, Hou-Zheng Xiang, Zhan-Guo Zhang, Koji Kuramoto, and Ai-Lin Xia, "Facile synthesis and ferrimagnetic property of spinel $(CoCrFeMnNi)_3O_4$ high-entropy oxide nanocrystalline powder," Journal of Molecular Structure **1194**, 11–18 (2019).

[26] Zbigniew Grzesik, Grzegorz Smoła, Maria Miszczak, Mirosław Stygar, Juliusz Dąbrowa, Marek Zajusz, Konrad Świerczek, and Marek Danielewski, "Defect structure and transport properties of $(Co,Cr,Fe,Mn,Ni)_3O_4$ spinel-structured high entropy oxide," Journal of the European Ceramic Society **40**, 835–839 (2020).

[27] Chih-Yang Huang, Chun-Wei Huang, Min-Ci Wu, Jagabandhu Patra, Thi Xuyen Nguyen, Mu-Tung Chang, Oliver Clemens, Jyh-Ming Ting, Ju Li, Jeng-Kuei Chang, and Wen-Wei Wu, "Atomic-scale investigation of lithiation/delithiation mechanism in high-entropy spinel oxide with superior electrochemical performance," Chemical Engineering Journal **420**, 129838 (2021).

[28] Mirosław Stygar, Juliusz Dąbrowa, Maciej Moździerz, Marek Zajusz, Wojciech Skubida, Krzysztof Mroczka, Katarzyna Berent, Konrad Świerczek, and Marek Danielewski, "Formation and properties of high entropy oxides in Co-Cr-Fe-Mg-Mn-Ni-O system: Novel $(Cr,Fe,Mg,Mn,Ni)_3O_4$ and $(Co,Cr,Fe,Mg,Mn)_3O_4$ high entropy spinels," Journal of the European Ceramic Society **40**, 1644–1650 (2020).

[29] Thi Xuyen Nguyen, Jagabandhu Patra, Jeng-Kuei Chang, and Jyh-Ming Ting, "High entropy spinel oxide nanoparticles for superior lithiation–delithiation performance," J. Mater. Chem. A **8**, 18963–18973 (2020).

[30] Bhusankar Talluri, M.L. Aparna, N. Sreenivasulu, S.S. Bhattacharya, and Tiju Thomas, "High entropy spinel metal oxide $(CoCrFeMnNi)_3O_4$ nanoparticles as a high-performance supercapacitor electrode material," Journal of Energy Storage **42**, 103004 (2021).

[31] Dan Wang, Shunda Jiang, Chanqin Duan, Jing Mao, Ying Dong, Kangze Dong, Zhiyuan Wang, Shaohua Luo, Yanguo Liu, and Xiwei Qi, "Spinel-structured high entropy oxide $(FeCoNiCrMn)_3O_4$ as anode towards superior lithium storage performance," Journal of Alloys and Compounds **844**, 156158 (2020).

[32] Dongdong Wang, Zhijuan Liu, Shiqian Du, Yiqiong Zhang, Hao Li, Zhaohui Xiao, Wei Chen, Ru Chen, Yanyong Wang, Yuqin Zou, and Shuangyin Wang, "Low-temperature synthesis of small-sized high-entropy oxides for water oxidation," J. Mater. Chem. A **7**, 24211–24216 (2019).

[33] Abhishek Sarkar, Benedikt Eggert, Ralf Witte, Johanna Lill, Leonardo Velasco, Qingsong Wang, Janhavika Sonar, Katharina Ollefs, Subramshu S Bhattacharya, Richard A Brand, *et al.*, "Comprehensive investigation of crystallographic, spin-electronic and magnetic structure of $(Co_{0.2}Cr_{0.2}Fe_{0.2}Mn_{0.2}Ni_{0.2})_3O_4$: Unraveling the suppression of configuration entropy in high entropy oxides," Acta Materialia , 117581 (2021).

[34] P Garcia Casado and I Rasines, "Crystal data for the spinels MGa_2O_4 (M = Mg, Mn)," Zeitschrift für Kristallographie **160**, 33–37 (1982).

[35] J Ghose, G C Hallam, and D A Read, "A magnetic study of $FeGa_2O_4$," Journal of Physics C: Solid State Physics **10**, 1051–1057 (1977).

[36] Akihiko Nakatsuka, Yuya Ikeda, Noriaki Nakayama, and Tadato Mizota, "Inversion parameter of the $CoGa_2O_4$ spinel determined from single-crystal X-ray data," Acta Crystallographica Section E **62**, i109–i111 (2006).

[37] C. Otero Areán and M. C. Trobajo-Fernandez, "Cation distribution in $Mg_xNi_{1-x}Ga_2O_4$ oxide spinels," Physica Status Solidi (a) **92**, 443–447 (1985).

[38] Juan Rodríguez-Carvajal, "Recent advances in magnetic structure determination by neutron powder diffraction," Physica B: Condensed Matter **192**, 55–69 (1993).

[39] AS Wills, "A new protocol for the determination of magnetic structures using simulated annealing and representational analysis (SARAh)," Physica B: Condensed Matter **276**, 680–681 (2000).

[40] D. G. Hawthorn, F. He, L. Venema, H. Davis, A. J. Achkar, J. Zhang, R. Sutarto, H. Wadati, A. Radi, T. Wilson, G. Wright, K. M. Shen, J. Geck, H. Zhang, V. Novák, and G. A. Sawatzky, "An in-vacuum diffractometer for resonant elastic soft x-ray scattering," Review of Scientific Instruments **82**, 073104 (2011).

[41] Marius Retegan, "Crispy: v0.7.3," (2019).

[42] Cornelius Lanczos, "An iteration method for the solution of the eigenvalue problem of linear differential and integral operators," (1950).

[43] M. W. Haverkort, M. Zwierzycki, and O. K. Andersen, "Multiplet ligand-field theory using Wannier orbitals," Phys. Rev. B **85**, 165113 (2012).

[44] Myrtille O.J.Y. Hunault, Yoshihisa Harada, Jun Miyawaki, Jian Wang, Andries Meijerink, Frank M. F. de Groot, and Matti M. van Schooneveld, "Direct observation of Cr^{3+} $3d$ states in ruby: Toward experimental mechanistic evidence of metal chemistry," The Journal of Physical Chemistry A **122**, 4399–4413 (2018), pMID: 29660293.

[45] G van der Laan and I W Kirkman, "The 2p absorption spectra of 3d transition metal compounds in tetrahedral and octahedral symmetry," Journal of Physics: Condensed Matter **4**, 4189–4204 (1992).

[46] Michael Dettbarn, Volodymyr B. Zabolotnyy, Abdul V. Tcakaev, Ronny Sutarto, Feizhou He, Yunzhong Chen, Robert J. Green, and Vladimir Hinkov, "Strain induced stabilization of a static Jahn-Teller distortion in the O^*-phase of $La_{7/8}Sr_{1/8}MnO_3$," (2020), 10.48550/ARXIV.2011.07108.

[47] P. Ferriani, G. Ghiringhelli, G. Ferrari, C.M. Bertoni, A. Tagliaferri, L. Braicovich, and N.B. Brookes, "Resonant

inelastic x-ray scattering from magnetic systems: Mn in $MnFe_2O_4$," Nuclear Instruments and Methods in Physics Research Section B: Beam Interactions with Materials and Atoms **200**, 220–225 (2003).

[48] Hebatalla Elnaggar, RuPan Wang, Mahnaz Ghiasi, Maria Yañez, Mario U. Delgado-Jaime, Mai Hussein Hamed, Amélie Juhin, Sarnjeet S. Dhesi, and Frank de Groot, "Probing the local distortion of Fe sites in Fe_3O_4 thin films using enhanced symmetry selection in xmld," Phys. Rev. Materials **4**, 024415 (2020).

[49] Matti M. van Schooneveld, Reshmi Kurian, Amélie Juhin, Kejin Zhou, Justine Schlappa, Vladimir N. Strocov, Thorsten Schmitt, and Frank M. F. de Groot, "Electronic structure of CoO nanocrystals and a single crystal probed by resonant x-ray emission spectroscopy," The Journal of Physical Chemistry C **116**, 15218–15230 (2012).

[50] Milan Gacic, Gerhard Jakob, Christian Herbort, Hermann Adrian, Thomas Tietze, Sebastian Brück, and Eberhard Goering, "Magnetism of Co-doped ZnO thin films," Phys. Rev. B **75**, 205206 (2007).

[51] M. W. Haverkort, Z. Hu, J. C. Cezar, T. Burnus, H. Hartmann, M. Reuther, C. Zobel, T. Lorenz, A. Tanaka, N. B. Brookes, H. H. Hsieh, H.-J. Lin, C. T. Chen, and L. H. Tjeng, "Spin state transition in $LaCoO_3$ studied using soft x-ray absorption spectroscopy and magnetic circular dichroism," Phys. Rev. Lett. **97**, 176405 (2006).

[52] D. Alders, L. H. Tjeng, F. C. Voogt, T. Hibma, G. A. Sawatzky, C. T. Chen, J. Vogel, M. Sacchi, and S. Iacobucci, "Temperature and thickness dependence of magnetic moments in NiO epitaxial films," Phys. Rev. B **57**, 11623–11631 (1998).

[53] Satoshi Sasaki, Kiyoshi Fujino, and Yoshio Takéuchi, "X-ray determination of electron-density distributions in oxides, MgO, MnO, CoO, and NiO, and atomic scattering factors of their constituent atoms," Proceedings of the Japan Academy, Series B **55**, 43–48 (1979).

[54] We define T_C by a slope method wherein the approximately linear increase in the susceptibility is extrapolated to its x-intercept.

[55] Brianna Musicó, Quinton Wright, T Zac Ward, Alexander Grutter, Elke Arenholz, Dustin Gilbert, David Mandrus, and Veerle Keppens, "Tunable magnetic ordering through cation selection in entropic spinel oxides," Physical Review Materials **3**, 104416 (2019).

[56] J Cieslak, M Reissner, K Berent, J Dabrowa, M Stygar, M Mozdzierz, and M Zajusz, "Magnetic properties and ionic distribution in high entropy spinels studied by Mössbauer and ab initio methods," Acta Materialia **206**, 116600 (2021).

[57] F Scholl and Ko Binder, "Selective sublattice dilution in ordered magnetic compounds: A new kind of percolation problem," Zeitschrift für Physik B Condensed Matter **39**, 239–247 (1980).

[58] Y Yafet and Ch Kittel, "Antiferromagnetic arrangements in ferrites," Physical Review **87**, 290 (1952).

[59] NS Satya Murthy, MG Natera, SI Youssef, RJ Begum, and CM Srivastava, "Yafet-Kittel angles in zinc-nickel ferrites," Physical review **181**, 969 (1969).

[60] Matthew A Willard, Yuichiro Nakamura, David E Laughlin, and Michael E McHenry, "Magnetic properties of ordered and disordered spinel-phase ferrimagnets," Journal of the American Ceramic Society **82**, 3342–3346 (1999).

[61] Richard A.D. Pattrick, Gerrit Van Der Laan, C. Michael B. Henderson, Pieter Kuiper, Esther Dudzik, and David J. Vaughan, "Cation site occupancy in spinel ferrites studied by x-ray magnetic circular dichroism: developing a method for mineralogists," European Journal of Mineralogy **14**, 1095–1102 (2002).